AIAA JOURNAL
Vol. 44, No. 2, February 2006

Exact Solution for Multidimensional Compressible Reactive Flow for Verifying Numerical Algorithms

Joseph M. Powers*
University of Notre Dame, Notre Dame, Indiana 46556-5637
and
Tariq D. Aslam†
Los Alamos National Laboratory, Los Alamos, New Mexico 87545

A new exact solution of an oblique detonation is developed for the supersonic irrotational flow of an inviscid calorically perfect ideal gas, which undergoes a one-step, irreversible, exothermic, zero activation energy reaction as it passes through a straight shock over a curved wedge. The solution gives expressions for the velocity, pressure, density, temperature, and position as parametric functions of a variable characterizing the extent of reaction. For Chapman–Jouguet solutions, an explicit form with dependency on distance is obtained in terms of the Lambert *W* function. As the simple model employed is a rational limit of models used in the computational simulation of complex supersonic reactive flows, the solution can serve as a benchmark for mathematical verification of general computational algorithms. An example of such a verification is given by comparing the predictions a modern shock-capturing code to those of the full exact solution. The realized spatial convergence rate is 0.779, far less than the fifth-order accuracy that the chosen algorithm would exhibit for smooth flows, but consistent with the predictions of all shock-capturing codes, which never converge with greater than first-order accuracy for flows with embedded discontinuities.

Nomenclature

A = reactant
a_1 = intermediate constant, m
a_2 = intermediate constant
a_3 = intermediate constant
a_4 = intermediate constant
B = product
e = specific internal energy, J/kg
H = Heaviside function
i = discrete cell counter
j = discrete cell counter
L_1 = absolute value norm of density error, kg/m
M = Mach number
N = number of points -1 in a given direction
p = pressure, Pa
q = specific heat release, J/kg
R = gas constant, J/kg $\cdot$ K^{-1}
s = dummy variable of integration
T = temperature, K
t = time, s
U = X-velocity component, m/s
u = x-velocity component, m/s
V = Y-velocity component, m/s
v = y-velocity component, m/s
W = Lambert product-log function
w = dummy variable
X = rotated distance coordinate, m
x = distance coordinate, m
Y = rotated distance coordinate, m
Y_A = mass fraction of reactant
Y_B = mass fraction of product
y = distance coordinate, m
α = reaction kinetic rate constant, 1/s
β = shock angle, rad
γ = ratio of specific heats
λ = reaction progress
ρ = density, kg/m^3
ψ = level set function
ω = vorticity, 1/s

Subscripts

CJ = Chapman–Jouguet
e = exact
i = ignition
n = numerical
r = reaction zone
s = streamline
w = wall
0 = point on shock surface
1 = unshocked freestream

I. Introduction

A. Verification

COMPUTATIONAL methods are increasingly being employed throughout the design process of a variety of aerospace applications, including those involving supersonic reactive flow with embedded shock waves, which are the topics of study here. For the engineering community to have confidence in these predictive tools, it is necessary for the predictions to be both verified and validated.[1–3] Verification indicates the computational algorithm is converging to the solution of the underlying mathematical model. Generally, verification is achieved when a computational scheme, which satisfies the traditional notions of consistency and numerical stability,[4] can be shown to be converging at a proper rate to a benchmark solution. The more difficult process of validation connotes that the underlying mathematical model captures the essence of experimental observation.

Although both verification and validation are necessary, this study will focus on verification alone. To enable a more robust verification

Received 3 November 2004; presented as Paper 2005-1173 at the AIAA 43rd Aerospace Sciences Meeting, Reno, NV, 10–13 January 2005; revision received 16 June 2005; accepted for publication 15 August 2005.

*Associate Professor, Department of Aerospace and Mechanical Engineering; powers@nd.edu. Associate Fellow AIAA.
†Technical Staff Member, Detonation Physics Team; aslam@lanl.gov.

than can be obtained by traditional known inert and one-dimensional solutions, a new benchmark exact solution for a supersonic reactive flow known as an oblique detonation will be identified. The solution contains the features of simplicity, two-dimensionality, an embedded shock, and a reaction zone of finite thickness, which should render it an attractive option for use in verifying numerical algorithms. In particular, the solution is not burdened with zones of numerical viscosity, which can easily corrupt predictions of fine-scale reaction zone lengths. The solution, that will be seen to give predictions consistent with notions that have evolved over the past several decades, does not significantly alter the standard understanding of oblique detonations. Moreover, the significant assumptions required do not render the reduced model appropriate to quantitatively describe an actual laboratory experiment; thus, no validation will be reported here. However, in addition to its value as a verification tool, there is a pedagogical advantage to be realized in constructing simplified exact solutions: one learns to distinguish the critical ingredients necessary to achieve an oblique detonation from those that provide higher-order corrections.

It is unfortunately easy to find in the literature widespread use of unverified and inaccurate computational predictions of similar flows. For example, using a one-dimensional framework, Powers and Paolucci[5] identify several modern calculations of detonations with detailed chemical kinetics, that were predicted on grids that were up to four orders of magnitude too coarse to capture the reaction zone structures intrinsic to the chemistry embodied in the underlying mathematical model. In such underresolved calculations, spurious effects of numerical viscosity are dominant at the finest length scales, and these are likely suppressing potentially important physical effects, especially near physical stability limits.

In a two-dimensional framework, the challenges are greater. With simple one-step kinetics, Wescott et al.[6] required a discretization of the reaction zone into 20 cells in the half-reaction zone length to generate an accurate numerical prediction of a detonation wave turning a corner. In a related calculation, Bdzil et al.[7] report "substantial differences in computed wave speed with resolution." Oran and Sichel[8] were able to sufficiently resolve their calculations with a two-step kinetic model of H_2-O_2 combustion to predict experimental data of detonation diffraction; whether such success could be achieved with a detailed kinetics model is questionable given present computational resources. Additional studies that show effects of numerical resolution in detonation diffraction along with some striking results are given by Arienti and Shepherd[9] and Helzel et al.[10]

For such problems, two classes of length scales need be resolved: 1) those associated with reaction zone kinetics and 2) a radius of curvature scale; moreover, there must be sufficient resolution to suppress the effect of algorithm-induced length scales that arise from numerical viscosity. Only when both classes of physical scales are captured and dominate the discretization-induced scale is the diffraction process correctly predicted. It is not difficult to identify studies of multidimensional detonation that do not meet this exacting standard.[5]

B. Oblique Detonation

An oblique detonation is defined as a shock-induced combustion process in which the shock has a nonnormal angle of inclination to the streamlines of the undisturbed flow. In a detonation, the shock triggers the combustion, and the combustion contributes to the support of the shock. It is generally the case that convective transport dominates diffusive transport. In a typical oblique detonation, an unreacted fluid particle traveling at supersonic velocity in the freestream encounters an oblique shock. Typically, the shock is supported by a stationary downstream solid wedge. As the fluid particle passes through the shock, it is irreversibly compressed such that its temperature rises sufficiently high to induce exothermic reaction. As the particle travels past the shock, it reacts, converting chemical energy into thermal and kinetic energy. This local energy release then propagates via acoustic waves within the domain between the wedge and the shock, and there is a complex series of reflections and interactions. Additionally, the fluid particle turns so that in the far field its pathline is parallel to the supporting wedge. An observable global consequence of this energy release and transport is that the shock is displaced further from the wedge than it otherwise would have been had the flow been inert.

The just-described portrait of an oblique detonation is qualitatively consistent with both experiments and a mathematical theory that has been refined over the past 60 years. Here a small portion of the theoretical literature that is most relevant to the present effort is reviewed. Early analyses focused on the limit of infinitely fast kinetic rates, which allowed an oblique detonation to be modeled by a set of algebraic Rankine–Hugoniot jump conditions with heat release, which gave rise to a prediction of a straight shock attached to a straight wedge. Such an oblique detonation has an infinitely thin reaction zone and can be thought of as structure free. Perhaps the first analysis of this type published in the open literature was given by Samaras.[11] Later, Gross[12] improved upon this to obtain a compact and useful representation of the oblique detonation jump state. Pratt et al.'s[13] revisitation of the structure-free problem in many ways triggered a renewed interest in oblique detonations for propulsion applications.

In an exothermic analog to the related study of Lee,[14] who considered flows with finite-rate vibrational relaxation, Powers and Stewart[15] extended the structure-free theory to account for the effects of a single reaction with finite-rate kinetics in the limit in which the flow kinetic energy is large relative to the chemical and ambient thermal energies. A special nonorthogonal coordinate system was used to facilitate their asymptotic analysis. Comparisons of the predictions of this theory with those of a standard algorithm for solving the full partial differential equations were given by Grismer and Powers[16] for the case of a curved shock attached to a straight wedge. Using an orthogonal coordinate transformation, Powers and Gonthier[17] extended this theory to account for two finite-rate reactions for a straight shock, curved wedge system. Grismer and Powers[18] went on to use an unsteady two-dimensional reactive Euler model to computationally predict stable and unstable oblique detonations with a straight shock and curved wedge.

These solutions, useful as verification tools, have not been widely utilized in the decade since they appeared. Three factors have likely inhibited the adaptation of the asymptotic solution as a verification benchmark: 1) the asymptotic solution for the curved shock and straight wedge has an elaborate form; 2) one must use great care to distinguish errors of the asymptotic approximation from numerical truncation errors; and 3) a realization of the often-critical need for verified computational tools, as embodied for example in AIAA standards on numerical accuracy, has not permeated throughout the aerospace community. The present study is an attempt to address these shortcomings.

C. Plan of the Paper

The plan of this paper is as follows. We first describe an unsteady, two-dimensional, inviscid model equivalent to that of Ref. 15. Reaction is described by one-step, irreversible kinetics, which allows for reactant depletion to extinguish the reaction. Arrhenius effects are embodied in a Heaviside step function, which suppresses reaction before the shock and admits reaction following the shock. Consequently the postshock reaction is equivalent to an Arrhenius model with zero activation energy. This key assumption allows the equations to be more amenable to analytic solution and the steady solutions to be less susceptible to instability. Next an orthogonal coordinate transformation is employed in a manner similar to that used in Ref. 17. The flow is taken to be steady and have spatial variation with only one of the variables in the transformed frame. This, along with the assumption of a straight shock attached to a curved wedge, dictates that the flow is irrotational. The conservation of mass, momentum, and energy equations is then seen to admit algebraic solutions, similar to Rankine–Hugoniot relations, which allows one to express all variables as functions of the extent of reaction. These are deployed in the remaining ordinary differential equation for the reaction kinetics, whose simple form admits then an exact solution giving distance as a function of extent of reaction. Consequently, all flow variables have a parametric expression in terms of the extent of reaction. The exact solution is then

employed for use in verification of a modern computational algorithm for shock-laden reactive flows. It is shown that a third-order time-accurate numerical algorithm, which can achieve fifth-order spatial accuracy for smooth flows, converges at less than first-order spatial accuracy for a flow containing a captured shock. This result is a feature of all shock-capturing schemes and is consistent with Godunov's theorem,[19] which formally applies only to linear algorithms, in contrast to the nonlinear method employed here.

II. Governing Equations

A. Evolution Axioms and Constitutive Equations

The two-dimensional unsteady reactive Euler equations for a calorically perfect ideal gas that undergoes a single irreversible reaction are expressed in conservative form as

$$\frac{\partial \rho}{\partial t} + \frac{\partial}{\partial x}(\rho u) + \frac{\partial}{\partial y}(\rho v) = 0 \tag{1}$$

$$\frac{\partial}{\partial t}(\rho u) + \frac{\partial}{\partial x}(\rho u^2 + p) + \frac{\partial}{\partial y}(\rho uv) = 0 \tag{2}$$

$$\frac{\partial}{\partial t}(\rho v) + \frac{\partial}{\partial x}(\rho uv) + \frac{\partial}{\partial y}(\rho v^2 + p) = 0 \tag{3}$$

$$\frac{\partial}{\partial t}\left\{\rho\left[e + \frac{1}{2}(u^2+v^2)\right]\right\} + \frac{\partial}{\partial x}\left\{\rho u\left[e + \frac{1}{2}(u^2+v^2) + \frac{p}{\rho}\right]\right\} + \frac{\partial}{\partial y}\left\{\rho v\left[e + \frac{1}{2}(u^2+v^2) + \frac{p}{\rho}\right]\right\} = 0 \tag{4}$$

$$\frac{\partial}{\partial t}(\rho\lambda) + \frac{\partial}{\partial x}(\rho u\lambda) + \frac{\partial}{\partial y}(\rho v\lambda) = \alpha\rho(1-\lambda)H(T - T_i) \tag{5}$$

$$e = \frac{1}{\gamma - 1}\frac{p}{\rho} - \lambda q \tag{6}$$

$$p = \rho RT \tag{7}$$

Equations (1–7) form a set of seven equations in the seven unknowns ρ, u, v, p, e, λ, and T. Here, as indicated in Fig. 1, the ordinary Cartesian distance coordinates are x and y. Dependent variables in Eqs. (1–7) are density ρ, x velocity u, y velocity v, pressure p, specific internal energy e, reaction progress λ, and temperature T. Parameters are the reaction kinetic rate constant α, ratio of specific heats γ, heat release per unit mass q, gas constant R, and ignition temperature T_i.

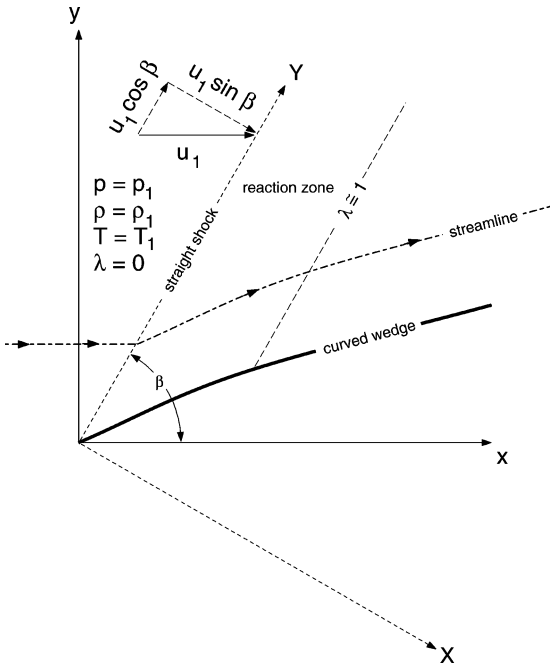

Fig. 1 Schematic of configuration for straight-shock, curved wedge oblique detonation.

Equations (1–5) are, respectively, expressions of the conservation of mass, x momentum, y momentum, and energy, and species evolution. Equation (5) models the irreversible reaction of $A \rightarrow B$ in which species A and B have identical molecular masses and specific heats. The mass fractions of each species Y_A and Y_B can be given in terms of the reaction progress variable by the relations $Y_A = 1 - \lambda$ and $Y_B = \lambda$. For a fluid particle that is initially composed exclusively of species A and reacts until it is exclusively composed of species B, one has λ beginning at zero and terminating at unity. The reaction rate is limited by a reactant depletion model and is proportional to the amount of reactant present. In Eq. (5), $H(T - T_i)$ is a Heaviside step function, which suppresses reaction when the temperature is below T_i; this mimics a full Arrhenius model, in which the activation energy is infinite for $T < T_i$ and zero for $T > T_i$. Equations (6) and (7) are constitutive relations that give the caloric and thermal state equations, respectively. Also useful will be the expression for total and component Mach numbers

$$M = \sqrt{(u^2+v^2)/(\gamma RT)}, \qquad M_x = u\Big/\sqrt{\gamma RT}$$
$$M_y = v\Big/\sqrt{\gamma RT} \tag{8}$$

and the vorticity ω, which for this two-dimensional flow has only one nonzero scalar component,

$$\omega = \frac{\partial v}{\partial x} - \frac{\partial u}{\partial y} \tag{9}$$

B. Freestream, Shock, and Boundary Conditions

Here, freestream, shock, and boundary conditions are given for Eqs. (1–7). As only time-independent solutions will be considered, a set of initial conditions is unnecessary. As indicated in Fig. 1, the scenario of a uniform supersonic freestream encountering a straight shock will be modeled. The shock is inclined at an angle β to the horizontal. The freestream variables have values

$$u = u_1, \qquad v = 0, \qquad \rho = \rho_1, \qquad T = T_1, \qquad \lambda = 0 \tag{10}$$

Then by Eq. (7), the ambient pressure is $p_1 = \rho_1 RT_1$, and by Eq. (8) the freestream Mach number is $M_1 = u_1/\sqrt{(\gamma RT_1)}$.

A standard Rankine–Hugoniot analysis reveals that λ does not jump through a shock discontinuity. This is understandable when one considers that a fluid particle needs a finite amount of time to react and that it spends an infinitesimally short time traversing the shock jump. The shock jump is taken to be of sufficient strength to raise the temperature above T_i, so as to cause reaction to commence. Thus in the postshock state, the Heaviside function in Eq. (5) has value unity and will not be written explicitly from here on. One can also write a detailed set of Rankine–Hugoniot shock jump equations for the other conservation relations; however, because the governing equations are already in the required conservative form, they are entirely consistent with the more general analysis that will follow.

Streamlines $y_s(x)$, which for the steady flow are also particle pathlines, must satisfy the standard equation

$$\frac{\mathrm{d}y_s}{\mathrm{d}x} = \frac{v}{u} \tag{11}$$

along with an appropriate initial condition. The shock is assumed to be straight and is taken to be attached to a downstream wall of shape $y = y_w(x)$. The wall shape necessary to induce a straight shock is as of yet unknown and will be determined as part of the solution procedure. For the inviscid flow, it is not necessary to satisfy a no-slip condition at the downstream wall. It is however necessary to satisfy a kinematic condition that allows no mass flow through the wall surface. This will be guaranteed if the wall surface is coincident with a streamline, so that

$$\frac{\mathrm{d}y_w}{\mathrm{d}x} = \frac{v}{u}, \qquad y_w(0) = 0, \qquad \text{on} \qquad y = y_w(x) \tag{12}$$

III. Exact Solution

In this section, an exact oblique detonation solution, which is appropriate for use in verification studies, is found.

A. Rotation of Axes

One first considers the rotation sketched in Fig. 1. Equations (1–5) are invariant under a clockwise rotation of axes through an angle $\pi/2-\beta$. If $\beta=\pi/2$ is selected, there is no rotation, and all results obtained here will be valid for the important limit of a strictly one-dimensional detonation. The rotation transformation is effected by the area-preserving linear mappings

$$X = x\sin\beta - y\cos\beta \tag{13}$$

$$Y = x\cos\beta + y\sin\beta \tag{14}$$

$$U = u\sin\beta - v\cos\beta \tag{15}$$

$$V = u\cos\beta + v\sin\beta \tag{16}$$

Here X and Y are the distance components in the rotated coordinate system, and U and V are the corresponding velocity components.

A critical advantage of such a rotation is that in the rotated frame the shock locus has the straightforward description $X=0$. It is also easily seen that magnitudes of distances and velocities are preserved under these transformations, that is, $x^2+y^2=X^2+Y^2$ and $u^2+v^2=U^2+V^2$. Further, scalars such as p, ρ, e, and λ are also invariant under the transformation. Thus, freestream scalars remain unchanged; however, the freestream velocity components transform to $U_1=u_1\sin\beta$, $V_1=u_1\cos\beta$. Equations for streamlines originating at a generic point on the shock surface $X=0, Y=Y_0$ transform to

$$\frac{\mathrm{d}Y_s}{\mathrm{d}X}=\frac{V}{U}, \qquad Y_s(0)=Y_0 \tag{17}$$

For the streamline at the wall, $Y_0=0$, and the downstream wall condition, Eq. (12), transforms to

$$\frac{\mathrm{d}Y_w}{\mathrm{d}X}=\frac{V}{U}, \qquad Y_w(0)=0, \qquad \text{on} \qquad Y=Y_w(X) \tag{18}$$

We seek solutions that have no variation in Y or t. In the rotated coordinate system in these limits, Eqs. (1–5) reduce to

$$\frac{\mathrm{d}}{\mathrm{d}X}(\rho U)=0 \tag{19}$$

$$\frac{\mathrm{d}}{\mathrm{d}X}(\rho U^2+p)=0 \tag{20}$$

$$\frac{\mathrm{d}}{\mathrm{d}X}(\rho UV)=0 \tag{21}$$

$$\frac{\mathrm{d}}{\mathrm{d}X}\left\{\rho U\left[e+\frac{1}{2}(U^2+V^2)+\frac{p}{\rho}\right]\right\}=0 \tag{22}$$

$$\frac{\mathrm{d}}{\mathrm{d}X}(\rho U\lambda)=\alpha\rho(1-\lambda) \tag{23}$$

Finally, the Mach numbers and vorticity transform to

$$M=\sqrt{\frac{U^2+V^2}{\gamma RT}}, \quad M_X=\frac{U}{\sqrt{\gamma RT}}, \quad M_Y=\frac{V}{\sqrt{\gamma RT}} \tag{24}$$

$$\omega=\frac{\mathrm{d}V}{\mathrm{d}X} \tag{25}$$

B. Extended Rankine–Hugoniot Conditions

Here, a set of algebraic equations, which are extensions of the standard Rankine–Hugoniot jump conditions, is obtained. Now, Eqs. (19–22) are homogeneous and can be directly integrated to arrive at a set of equations consistent with Rankine–Hugoniot jump conditions. Doing this, applying freestream conditions, Eq. (10), using Eq. (6) to eliminate e, and using Eq. (19) to simplify Eq. (23), one finds

$$\rho U=\rho_1 u_1\sin\beta \tag{26}$$

$$\rho U^2+p=\rho_1 u_1^2\sin^2\beta+p_1 \tag{27}$$

$$V=u_1\cos\beta \tag{28}$$

$$\frac{\gamma}{\gamma-1}\frac{p}{\rho}-\lambda q+\frac{1}{2}\left(U^2+u_1^2\cos^2\beta\right)=\frac{\gamma}{\gamma-1}\frac{p_1}{\rho_1}+\frac{1}{2}u_1^2 \tag{29}$$

$$\frac{\mathrm{d}\lambda}{\mathrm{d}X}=\alpha\frac{1-\lambda}{U} \tag{30}$$

Equation (28) is consistent with the well-known result from inert oblique shock theory that the velocity component tangent to the oblique shock is unchanged through the shock. But here the condition is stronger, as our assumptions give the result that V remains constant throughout the postshock reactive flowfield. Because V is constant, Eq. (25) holds that the entire postshock flowfield must be irrotational: $\omega=0$.

Equations (26–29) have full equivalents in Refs. 11–13, 15, and 17, albeit in slightly different notation. Now Eqs. (26), (27), and (29) constitute three nonlinear algebraic equations in the four unknowns ρ, U, p, and λ. A lengthy series of operations on these equations leads one to form an explicit algebraic expression for $\rho(\lambda)$:

$$\rho(\lambda)=\frac{\rho_1(\gamma+1)M_1^2\sin^2\beta}{1+\gamma M_1^2\sin^2\beta\pm\sqrt{\left(1+\gamma M_1^2\sin^2\beta\right)^2-(\gamma+1)M_1^2\sin^2\beta\left\{2+[(\gamma-1)/\gamma](2\lambda q/RT_1)+(\gamma-1)M_1^2\sin^2\beta\right\}}} \tag{31}$$

Now for a physical density prediction, the term inside the radical in Eq. (31) must be nonnegative for $\lambda\in[0,1]$. Algebraic analysis reveals that this condition will hold if

$$q\le\frac{\gamma RT_1\left(M_1^2\sin^2\beta-1\right)^2}{2(\gamma^2-1)M_1^2\sin^2\beta} \tag{32}$$

When the equality holds, the condition is the two-dimensional equivalent of a Chapman–Jouguet (CJ) detonation. The CJ oblique detonation given by this model can be shown to predict a locally sonic component of velocity normal to the oblique shock at the point of complete reaction ($\lambda=1$).

It can be shown that the $+$ solution of Eq. (31) is associated with the unshocked branch and the $-$ solution is associated with the shocked branch. More specifically, when $\lambda=0$, the $+$ solution is the ambient density ρ_1, and the $-$ solution is the classical inert oblique shock solution. As the unshocked branch has no clear mechanism to trigger ignition, it will be discarded from here on. The shocked $-$ branch of Eq. (31) is valid for the domain between the shock and the confining wall. It is a function of known freestream parameters and the as of yet unknown function $\lambda(X)$. Other variables are then easy to calculate. For example, using Eqs. (7), (26), and (27) one obtains

$$U(\lambda)=\frac{\rho_1 u_1\sin\beta}{\rho(\lambda)} \tag{33}$$

$$p(\lambda)=p_1+\rho_1^2u_1^2\sin^2\beta\left[\frac{1}{\rho_1}-\frac{1}{\rho(\lambda)}\right] \tag{34}$$

$$T(\lambda) = \frac{p_1}{\rho(\lambda)R} + \frac{\rho_1^2 u_1^2 \sin^2\beta}{\rho(\lambda)R}\left[\frac{1}{\rho_1} - \frac{1}{\rho(\lambda)}\right] \tag{35}$$

C. Reaction Zone Structure Solution

Now, the necessary ingredients are available for integration of Eq. (30). Employing Eq. (33), Eq. (30) can be rewritten as

$$\frac{\mathrm{d}\lambda}{\mathrm{d}X} = \frac{\alpha}{\rho_1 u_1 \sin\beta}\rho(\lambda)(1-\lambda), \qquad \lambda(0) = 0 \tag{36}$$

where $\rho(\lambda)$ is taken from the shocked $-$ branch of Eq. (31). Next separation of variables allows Eq. (36) to be integrated to form an exact solution for $X(\lambda)$:

$$X(\lambda) = a_1\left(2a_3\left(\sqrt{1-a_4\lambda}-1\right) + \ell n\left(\left(\frac{1}{1-\lambda}\right)^{a_2} \times \left\{\frac{\left[1-\sqrt{(1-a_4\lambda)/(1-a_4)}\right]\left[1+\sqrt{1/(1-a_4)}\right]}{\left[1+\sqrt{(1-a_4\lambda)/(1-a_4)}\right]\left[1-\sqrt{1/(1-a_4)}\right]}\right\}^{a_3\sqrt{1-a_4}}\right)\right) \tag{37}$$

where the intermediate parameters $a_1, \ldots, a_4$ have the definitions

$$a_1 = \frac{1}{(\gamma+1)M_1\sin\beta}\frac{\sqrt{\gamma RT_1}}{\alpha} \tag{38}$$

$$a_2 = 1 + \gamma M_1^2 \sin^2\beta \tag{39}$$

$$a_3 = M_1^2\sin^2\beta - 1 \tag{40}$$

$$a_4 = 2\frac{M_1^2\sin^2\beta}{\left(M_1^2\sin^2\beta - 1\right)^2}\frac{\gamma^2-1}{\gamma}\frac{q}{RT_1} \tag{41}$$

Note that a_1 has units of length and a_2, a_3, and a_4 are dimensionless. When $a_4 < 1$, Eq. (32) is satisfied, and Eq. (37) predicts a real solution. For $a_4 = 1$, a CJ oblique detonation is predicted. If $a_4 > 1$, Eq. (32) is violated, and complex values of X are predicted. Numerical experiments on Eq. (37) indicate that for $\lambda \in [0, 1]$ that $X(\lambda)$ is single valued and monotonically increasing with λ. When nonphysical large negative values of λ are considered, the function can be multivalued.

One can find the locus of a generic streamline Y_s originating at the shock surface $X = 0$, $Y = Y_0$ as a function of λ. Scaling Eq. (17) by Eq. (30) and employing Eq. (28), one gets

$$\frac{\mathrm{d}Y_s}{\mathrm{d}\lambda} = \frac{u_1\cos\beta}{\alpha}\frac{1}{1-\lambda}, \qquad Y_s(\lambda = 0) = Y_0 \tag{42}$$

Solving, one gets

$$Y_s(\lambda) = (u_1\cos\beta/\alpha)\,\ell n[1/(1-\lambda)] + Y_0 \tag{43}$$

For the streamline originating at the wall $Y_0 = 0$, the wall shape is given by

$$Y_w(\lambda) = (u_1\cos\beta/\alpha)\,\ell n[1/(1-\lambda)] \tag{44}$$

A detailed asymptotic analysis[20] for the limit in which the chemical energy is small relative to the kinetic energy shows that the order of magnitude of the reaction zone thickness X_r is well estimated by

$$X_r \sim \frac{\gamma-1}{\gamma+1}\frac{u_1\sin\beta}{\alpha} \times \left[1 + \frac{2}{(\gamma-1)M_1^2\sin^2\beta} + \frac{\gamma+1}{\gamma\left(M_1^2\sin^2\beta - 1\right)}\frac{q}{RT_1}\right] \tag{45}$$

D. CJ Case

When the flow conditions are such that $a_4 = 1$, the oblique detonation has a CJ character. The fluid velocity normal to the shock at the end of such a reaction zone is locally sonic; moreover, one set of characteristic curves becomes parallel to the shock wave. In a one-dimensional flow with one-step irreversible kinetics, the CJ velocity can be shown to be the velocity of an unsupported wave, and thus it has an important physical significance. In contrast, there is no particular tendency for most oblique detonations to relax to the CJ state; in practice, they are usually overdriven. However, because a new result is obtained, which is useful in the important one-dimensional limit, $\beta \to \pi/2$, a brief characterization of the CJ state is given here.

For $a_4 = 1$, Eq. (37) reduces considerably to

$$X_{\mathrm{CJ}}(\lambda) = -a_1\left[2a_3\left(1-\sqrt{1-\lambda}\right) + a_2\,\ell n(1-\lambda)\right] \tag{46}$$

Equation (46) can be inverted to form an explicit expression for $\lambda_{\mathrm{CJ}}(X)$:

$$\lambda_{\mathrm{CJ}}(X) = 1 - \left\{\frac{a_2}{a_3}W_0\left[-\frac{a_3}{a_2}\exp\left(-\frac{X}{2a_1a_2} - \frac{a_3}{a_2}\right)\right]\right\}^2 \tag{47}$$

Here, $W_0(s)$ is the principal branch of the Lambert W function,[21] of the dummy variable s. When $s = we^w$, $W(s) = w$, where w is also a dummy variable; consequently, W can be thought of as an extended logarithm, sometimes called the "product log." For $s \in [-e^{-1}, 0]$, as the argument is in Eq. (47), $W(s)$ is dual valued with both values negative. The principal branch $W_0(s)$ is taken as the branch, which has an analytic continuation through the origin. On the principal branch $s \in [-e^{-1}, 0]$ maps to $W_0 \in [-1, 0]$. The alternate branch $W_{-1}(s)$ is the branch that has an analytic continuation to negative infinity and maps $s \in [-e^{-1}, 0]$ onto $W_{-1} \in [-1, -\infty)$. For $s > 0$, $W(s)$ is single valued, and for $s < -e^{-1}$, $W(s)$ has no real value.

With $\lambda_{\mathrm{CJ}}(X)$ from Eq. (47), it is easy to predict the variation of other flow variables under CJ conditions using Eqs. (3), and (33–35). The CJ reaction zone thickness is estimated by taking $X_{\mathrm{rCJ}} \sim 2a_1a_2$. Using Eqs. (38) and (39), this reduces to

$$X_{\mathrm{rCJ}} \sim [2\gamma/(\gamma+1)](u_1\sin\beta/\alpha)\left[1 + 1\Big/\left(\gamma M_1^2\sin^2\beta\right)\right] \tag{48}$$

Last, one notes when $a_4 = 1$, that M_1 and q are no longer independent by Eq. (41). Solving for M_1 in terms of q for the CJ limit gives rise to a quartic equation, which has four complicated solutions for left and right running CJ deflagrations and detonations.

E. Predictions of the Exact Solution

A simple non-CJ test case is studied for a set of parameter values listed in Table 1. The numbers here are in infinite precision to facilitate the formal verification. The larger the value of q that is employed, the easier it is to visualize the effects of the heat release on the flowfield. Here $q = 300{,}000$ J/kg meets the additional restriction of Eq. (32), which for the parameters of Table 1 demand that $q \le 3{,}515{,}750/11$ J/kg; using the nomenclature described in Ref. 17,

Table 1 Parameters used in sample oblique detonation calculations

Parameter	Unit	Value
Independent		
R	J/kg · K^{-1}	287
α	1/s	1,000
β	rad	$\pi/4$
γ		6/5
T_1	K	300
M_1		3
ρ_1	kg/m^3	1
q	J/kg	300,000
Dependent		
u_1	m/s	$18\sqrt{2{,}870}$
p_1	Pa	86,100

Table 2 Solution values along the wall streamline for flow parameters of Table 1

λ	X, m	Y_w, m	x, m	y_w, m	p, Pa	T, K	ρ, kg/m^3
0.000000	0.000000	0.000000	0.000000	0.000000	86,100	300.000	1.00000
0.000000	0.000000	0.000000	0.000000	0.000000	414,845	423.416	3.41379
0.100000	0.021661	0.071842	0.066116	0.035483	406,941	439.454	3.22653
0.200000	0.047279	0.152154	0.141020	0.074158	398,616	455.334	3.05030
0.300000	0.078003	0.243204	0.227127	0.116815	389,794	471.027	2.88341
0.400000	0.115536	0.348314	0.327991	0.164599	380,374	486.496	2.72426
0.500000	0.162550	0.472633	0.449142	0.219261	370,215	501.688	2.57122
0.600000	0.223581	0.624787	0.599887	0.283695	359,111	516.525	2.42245
0.700000	0.307241	0.820947	0.797749	0.363245	346,734	530.883	2.27570
0.800000	0.433132	1.09742	1.08226	0.469723	332,510	544.549	2.12758
0.900000	0.664723	1.57005	1.58022	0.640165	315,234	557.069	1.97171
1.000000	∞	∞	∞	∞	291,192	567.048	1.78927

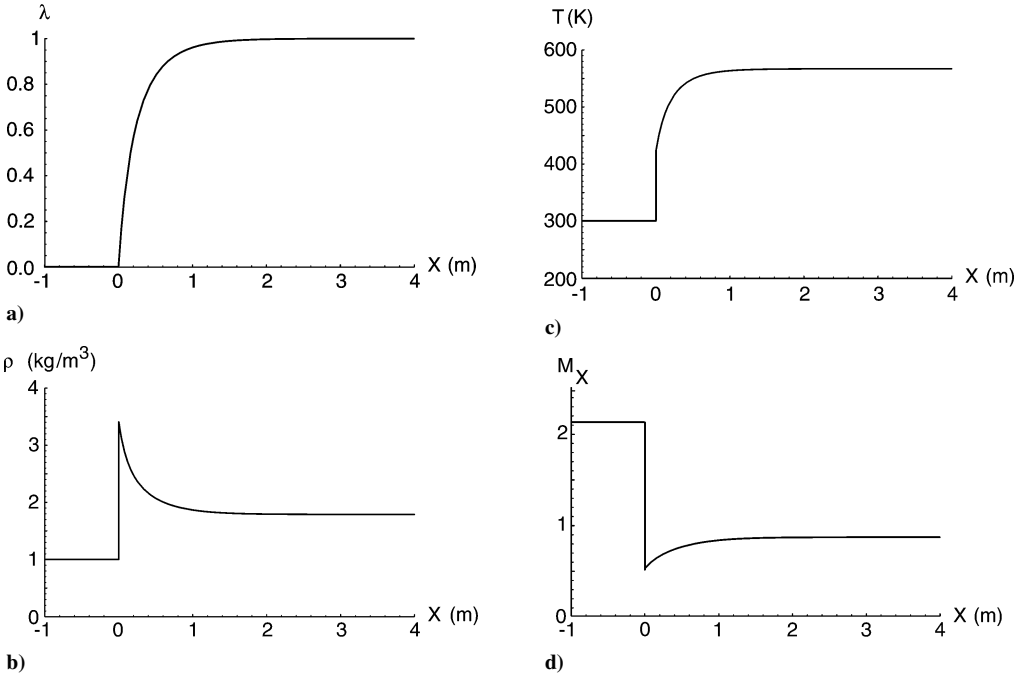

Fig. 2 Exact solution for flow variables: a) reaction progress, b) density, c) temperature, and d) Mach number normal to the shock, as function of normal distance from the shock X for parameters of Table 1.

this is an example of a weak overdriven oblique detonation. For $q > 3{,}515{,}750/11$ J/kg, a different class of flow topology would be predicted. For straightforward implementation into industrial codes, all parameters and results reported here are dimensional. These parameters, although somewhat arbitrary, are not unreasonable for common gases that might be operating in a high-speed propulsion device. In particular they were chosen so that the global reaction zone lengths were on the order of 1 m and that significant variation in flow variables, such as ρ and T, could be predicted throughout the reaction zone. It should be remembered, however, that the purpose of this paper is to develop a useful verification methodology utilizing the new exact solution; consequently, more flexibility in parameter choices is exercised relevant to the equally important, but distinct, task of validation relative to actual experiments.

In Fig. 2, a plot is given of various flow variables: reaction progress, density, temperature, and Mach number in the direction normal to the shock, as functions of the normal distance from the shock X. Figure 2a demonstrates that reaction progress is zero until the shock at $X = 0$ m is reached. At the shock, there is no jump in λ, whereas there is a jump in its derivative. The irreversible reaction induces a relaxation of λ to unity near $X = 0.6$ m. This agrees to the proper order of magnitude with the prediction of Eq. (45), which yields $X_r \sim 0.313$ m.

Figure 2b shows the variation of density. Here the shock jump is clearly seen at $X = 0$ m, followed by a relaxation to equilibrium in the reaction zone. In Fig. 2c, the temperature is seen to jump from its ambient value to over 423 K, which is followed by a further increase as heat is released until reaches an equilibrium value of near 567 K. The Mach number in the direction normal to the wave is initially supersonic at $M_X = M_1 \sin\beta = 3\sqrt{2}/2$. The shock jump reduces it to a subsonic state, and then it increases through the reaction zone to a final value of 0.862. Thus, this oblique detonation is, using nomenclature of Ref. 17, weak, in the sense of an oblique shock, and overdriven, in the sense of a detonation.

For use in a detailed flow verification of a computational code, a set of benchmark values along the wall streamline is given in Table 2. To perform a high-precision verification, as is reported in the section, many more points need to be considered. The truncated set given here simply provides the reader interested in performing independent verifications another means to check results. Although these predictions are valid for a single streamline, one can construct the entire flowfield by translating each streamline to a different origin on the oblique shock. This is a consequence of the solution only retaining variation in the X direction in the rotated coordinate system.

F. Numerical Algorithm

The numerical method employs a uniform Cartesian grid, with an internal boundary method to handle the curved wall boundary condition. The internal boundary is represented by a level set function $\psi = 0$, where $\psi > 0$ in the boundary region and $\psi < 0$

in the flow region. The computational domain is $x \in [x_{\min}, x_{\max}]$, $y \in [0, y_{\max}]$, with $x_{\min} < 0$, $x_{\max} > 0$, and the apex of the curved wedge at $(x, y) = (0, 0)$. The boundary conditions along $x = x_{\min}$ and $y = y_{\max}$ are such that all flow variables have zero gradient. Along $y = 0$ for $x \in [x_{\min}, 0]$, reflection boundary conditions are used. Above the wedge, along $x = x_{\max}$, zero-gradient boundary conditions are used. Note that if the shock exits the domain on the $x = x_{\max}$ boundary, the boundary conditions along $x = x_{\min}$, $y = 0$, and $y = y_{\max}$ are adequate. One has to ensure, however, a posteriori, that the flow characteristics are supersonic at the $x = x_{\max}$ boundary to utilize zero-gradient conditions at that boundary. The spatial discretization scheme is based on the nominally fifth-order weighted essentially nonoscillatory shock-capturing scheme of Jiang and Shu,[22] in conjunction with a nondecomposition-based Lax–Friedrichs solver. For temporal discretization, a third-order Runge–Kutta time-integration technique is used. The details are fully described in Xu et al.[23] It is emphasized that the fifth-order spatial accuracy can be realized only for flows that contain no discontinuities and for which no low-order boundary simulation errors are introduced, unlike those of this study. The physical parameters used in the computation are those in Table 1. In addition, the ignition temperature T_i is chosen to be halfway between the freestream and shock temperature $T_i = 361.58$ K.

G. Error Norm, Initial Conditions, and Time Integration

For verification, the exact solution must be compared with the computed one. When flows contain captured shocks, it is important to measure error using a norm such as L_1; for obvious reasons shock-capturing solutions will not converge in the L_∞ norm. The error in density, using an L_1 norm, is denoted by

$$L_1 = \sum_{i=0}^{N} \sum_{j=0}^{N} H(-\psi_{ij}) |\rho_{n,ij} - \rho_{e,ij}| \Delta x \Delta y \tag{49}$$

where ρ_n and ρ_e are the numerical and exact value of density, i and j are the grid indices, and $N+1$ is the number of points in either direction. Note that L_1, as defined, is dimensional with units of density $\times$ area. In all cases uniform grid sizes are utilized with $\Delta x = \Delta y$; from here on, only values for Δx will be reported. Here $H(-\psi_{ij})$ is the Heaviside function and is used so that errors are only measured in the flow region.

Because a time-dependent numerical algorithm is being used, initial conditions also need to be specified. These are simply given by the freestream conditions. When comparing a time-dependent numerical solution to a steady exact solution, it is imperative to consider a final time that is large enough to relax all physical transients. However, the computational predictions will never be exactly steady, so that the modeler must exercise some discretion in choosing when to terminate the calculation. In practice, it is not difficult to discern an appropriate cutoff time. It is also noted, making an inference from the study of Short and Stewart,[24] that it is likely that the exact physical solution is linearly stable to small perturbations because the zero activation energy case has been taken. So, when the time-dependent solution is near the steady, exact solution, all modes should decay exponentially in time to the steady, exact solution. So, for this problem, L_1 can be tracked as a function of time, and the solution is steady when L_1 is no longer significantly changing.

H. Predictions of the Computational Algorithm

A finite computational domain is considered with $x_{\min} = -\frac{1}{4}$ m, $x_{\max} = \frac{7}{4}$ m, $y_{\max} = 2$ m. As the exact solution is obtained on a semi-infinite spatial domain, additional error is potentially introduced by the finite truncation. Although this error has not been quantified, it is believed to be small: 1) as the domain length scaled by the characteristic reaction zone length, X_r is 6.4 so that the solution is essentially spatially relaxed; and 2) no characteristics at the right outflow boundary are pointing into the domain, thus preventing corruption of the solution from effects external to the computational domain.

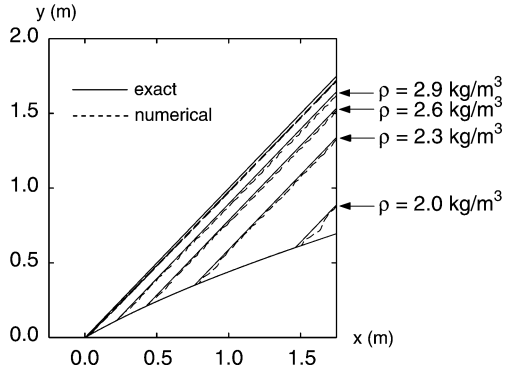

Fig. 3 Predictions of shock locus and density contours from exact and numerical approximation for parameters of Table 1 and 256 × 256 grid.

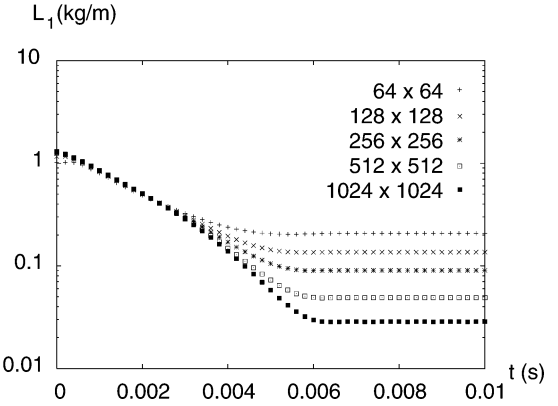

Fig. 4 L_1 residual norm for difference between predictions of density field from steady exact and time-dependent numerical methods as a function of time at several different grid resolutions for parameters of Table 1.

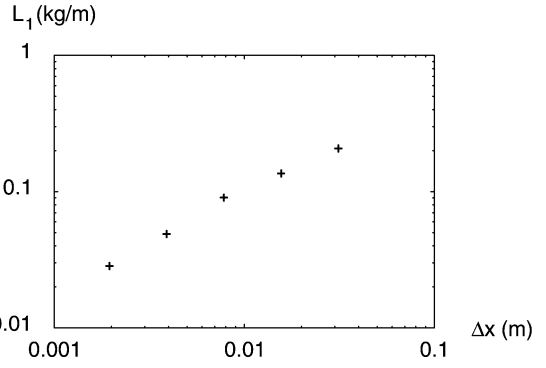

Fig. 5 L_1 error norm for difference between predictions of density field from exact and numerical methods in the long time limit as a function of grid size for parameters of Table 1; convergence rate $\sim \mathcal{O}(\Delta x^{0.779})$.

A comparison of exact and long time computed density contours is made in Fig. 3. Here a spatial discretization of $\Delta x = 1/128$ m was employed. There is good agreement between the predictions of the two methods. Figure 4 gives the L_1 residual in ρ as time advances for various spatial resolutions from $\Delta x = 1/32$ m to $\Delta x = 1/512$ m. The residuals, for all spatial resolutions, decrease rapidly at early time, and at nearly the same rate. When the residual starts to become time independent and thus represents the steady-state error, is a function of spatial resolution. This effect arises because the finer grid resolutions can faithfully track the time-dependent decaying modes further in time before being overwhelmed by the spatial inaccuracies. For example, the $\Delta x = 1/32$ m calculation appears to be steady around $t \approx 0.005$ s, whereas the $\Delta x = 1/512$ m calculation is not steady until $t \approx 0.006$ s. Figure 5 displays the L_1 error in density, at long time, vs grid discretization length. From this plot, it

is determined that the approximate rate of convergence in density is $\mathcal{O}(\Delta x^{0.779})$, nearly, but not quite, first order. The errors in other field variables show similar trends. The errors are likely attributable to the combined effects shock-capturing, level set wall boundary approximation, both of which are $O(\Delta x)$ accurate at best, and finite size of the computational domain. The sub-first-order convergence is typical of shock-capturing schemes where linearly degenerate characteristics exist, but is often missed when reporting convergence rates.

IV. Conclusions

A new exact solution, parameterized by reaction progress λ, for steady two-dimensional compressible reactive flow with a leading shock followed by a finite length reaction zone has been obtained. For a CJ detonation, the parametric form is unnecessary as one can go on to obtain an explicit representation of the flowfield as a function of position. Exact solutions for flows of this class are rare and have principal utility as benchmarks for verification of the predictions of computational codes. Here, with the employment of a modern shock-capturing code, an unambiguous example of a verification has been provided. The convergence study clearly illustrates that even though a nominally high-order discretization was employed inherent properties of the numerical scheme and limitations in finite approximations of a semi-infinite domain combine to suppress realization of high convergence rates when embedded discontinuities and complex boundaries are present. Although a formal stability analysis has not been performed for this steady solution, the fact that the unsteady numerical calculations relax to an apparently steady state gives strong indication that the results are indeed stable. This gives the solution even more value as a verification benchmark that can be exercised before proceeding on to simulation of the more challenging physically unstable detonation flows.

We envision the use of this solution in two ways. Perhaps most importantly, code developers can have a simple reliable solution against which to check if their code is capturing the leading-order features of a nontrivial problem. The key features of a resolved reaction zone structure and multidimensionality give an advantage over the typical verification solutions, which are usually confined to inert or one-dimensional problems. Second, the exact solution provides a means to precisely identify the sources of error for a given algorithm. For example, one could easily determine how the error behaves as one systematically shrinks the discretization length while holding the reaction zone length constant. Although this exercise is seemingly obvious, one must recall that it is rarely performed, and most modern calculations of detonations with detailed kinetics are in fact underresolved by many orders of magnitude.[5] Utilization of careful verification methods will allow a properly skeptical general community to have more trust in the predictions of computational modelers.

Acknowledgment

This study was performed under the auspices of the U.S. Department of Energy.

References

[1]Roache, P. J., "Quantification of Uncertainty in Computational Fluid Dynamics," *Annual Review of Fluid Mechanics*, Vol. 29, 1997, pp. 123–160.

[2]Oberkampf, W. L., and Trucano, T. G., "Verification and Validation in Computational Fluid Dynamics," *Progress in Aerospace Sciences*, Vol. 38, No. 3, 2002, pp. 209–272.

[3]Roy, C. J., "Review of Code and Solution Verification Procedures for Computational Simulation," *Journal of Computational Physics*, Vol. 205, No. 1, 2005, pp. 131–156.

[4]Hirsch, C., *Numerical Computation of Internal and External Flows*, Vol. 1, Fundamentals of Numerical Discretization, Wiley, New York, 1988, pp. 267–282.

[5]Powers, J. M., and Paolucci, S., "Accurate Spatial Resolution Estimates for Reactive Supersonic Flow with Detailed Chemistry," *AIAA Journal*, Vol. 43, No. 5, 2005, pp. 1088–1099.

[6]Wescott, B. L., Stewart, D. S., and Bdzil, J. B., "On Self-Similarity of Detonation Diffraction," *Physics of Fluids*, Vol. 16, No. 2, 2004, pp. 373–384.

[7]Bdzil, J. B., Aslam, T. D., Catanach, R. A., Hill, L. G., and Short, M., "DSD Front Models: Nonideal Explosive Detonation in ANFO," *Twelfth Symposium (International) on Detonation*, Office of Naval Research, ONR 333-05-2, Arlington, VA, 2002, pp. 409–417.

[8]Oran, E. S., and Sichel, M., "Insights into the Diffraction of Detonation Waves," *Computational Fluid Dynamics Journal*, Vol. 12, No. 2, 2003, pp. 242–247.

[9]Arienti, M., and Shepherd, J. E., "A Numerical Study of Detonation Diffraction," *Journal of Fluid Mechanics*, Vol. 529, 2005, pp. 117–146.

[10]Helzel, C., LeVeque, R. J., and Warnecke, G., "A Modified Fractional Step Method for the Accurate Approximation of Detonation Waves," *SIAM Journal on Scientific Computing*, Vol. 22, No. 4, 2000, pp. 1489–1510.

[11]Samaras, D. G., "Gas Dynamic Treatment of Exothermic and Endothermic Discontinuities," *Canadian Journal of Research A*, Vol. 26, No. 1, 1948, pp. 1–21.

[12]Gross, R. A., "Oblique Detonation Waves," *AIAA Journal*, Vol. 1, No. 5, 1963, pp. 1225–1227.

[13]Pratt, D. T., Humphrey, J. W., and Glenn, D. E., "Morphology of Standing Oblique Detonation Waves," *Journal of Propulsion and Power*, Vol. 7, No. 5, 1991, pp. 837–645.

[14]Lee, R. S., "A Unified Analysis of Supersonic Nonequilibrium Flow over a Wedge: I. Vibrational Nonequilibrium," *AIAA Journal*, Vol. 4, No. 1, 1966, pp. 30–37.

[15]Powers, J. M., and Stewart, D. S., "Approximate Solutions for Oblique Detonations in the Hypersonic Limit," *AIAA Journal*, Vol. 30, No. 3, 1992, pp. 726–736.

[16]Grismer, M. J., and Powers, J. M., "Comparisons of Numerical Oblique Detonation Solutions with an Asymptotic Benchmark," *AIAA Journal*, Vol. 30, No. 12, 1992, pp. 2985–2987.

[17]Powers, J. M., and Gonthier, K. A., "Reaction Zone Structures for Strong, Weak Overdriven, and Weak Underdriven Oblique Detonations," *Physics of Fluids A*, Vol. 4, No. 9, 1992, pp. 2082–2089.

[18]Grismer, M. J., and Powers, J. M., "Numerical Predictions of Oblique Detonation Stability Boundaries," *Shock Waves*, Vol. 6, No. 3, 1996, pp. 147–156.

[19]Godunov, S. K., "A Difference Scheme for Numerical Computation of Discontinuous Solutions of Hydrodynamic Equations," *Matematicheskii Sbornik*, Vol. 47, No. 3, 1959, pp. 271–306; English translation in U.S. Joint Publications Research Service, JPRS 7226, 1969.

[20]Powers, J. M., and Aslam, T. D., "Exact Solutions for Two-Dimensional Reactive Flow for Verification of Numerical Algorithms," AIAA Paper 2005-1173, Jan. 2005.

[21]Corless, R. M., Gonnet, G. H., Hare, D. E. G., Jeffrey, D. J., and Knuth, D. E., "On the Lambert *W* Function," *Advances in Computational Mathematics*, Vol. 5, No. 4, 1996, pp. 329–359.

[22]Jiang, G. S., and Shu, C. W., "Efficient Implementation of Weighted ENO Schemes," *Journal of Computational Physics*, Vol. 126, No. 1, 1996, pp. 202–228.

[23]Xu, S. J., Aslam, T., and Stewart, D. S., "High Resolution Numerical Simulation of Ideal and Non-Ideal Compressible Reacting Flows with Embedded Internal Boundaries," *Combustion Theory and Modelling*, Vol. 1, No. 1, 1997, pp. 113–142.

[24]Short, M., and Stewart, D. S., "Cellular Detonation Stability. Part 1. A Normal-Mode Linear Analysis," *Journal of Fluid Mechanics*, Vol. 368, 1998, pp. 229–262.

M. Sichel
Associate Editor